Acoustic mirage in two-dimensional gradient-index phononic crystals

Sz-Chin Steven Lin and Tony Jun Huang[a)]
Department of Engineering Science and Mechanics, The Pennsylvania State University, University Park, Pennsylvania 16802, USA

(Received 26 May 2009; accepted 5 August 2009; published online 15 September 2009)

We report the design of a two-dimensional gradient-index phononic crystal (GRIN PC) structure, which effectively demonstrates the "acoustic mirage" effect on the wavelength scale. Using the GRIN PC, the propagating direction of acoustic waves can be continuously bent along an arc-shaped trajectory by gradually tuning the filling ratio of PCs. We investigate the acoustic mirage effect through both plane wave expansion and finite-difference time-domain methods. By controlling the incident angle or operating frequency, the arc-shaped trajectory of acoustic wave propagation can be dynamically adjusted. The GRIN PC structure is composed of steel cylinders, positioned in a square lattice, and immersed in an epoxy. It can be fabricated through a simple process and seamlessly integrated with existing acoustic devices. In addition, we establish that such an acoustic effect can be used in the design of tunable acoustic waveguides, which could find applications in acoustic switching, filtering, and biosensing. © *2009 American Institute of Physics*.
[doi:10.1063/1.3213361]

I. INTRODUCTION

Understanding how waves bend under specific condition may reveal a new realm of effective optical/acoustical devices such as on-chip waveguides, filters, and multiplexers. As described by Snell's law, an atmospheric refractive-index gradient due to temperature variation can bend light waves to project a false image above or below a real object.[1] This phenomenon, known as the optical mirage, is analogous to the acoustic mirage where sound-speed gradients due to temperature, pressure, or salinity can guide acoustic waves traveling in seawater along a bowed trajectory toward lower sound-speed regions.[2] Originally only observed in nature on the kilometer scale due to the low gradient rate of refractive index or sound speed with respect to distance, recent studies, led by Centeno *et al.*,[3] demonstrated the optic mirage on the wavelength scale by introducing a sharp refractive-index gradient into the medium. With the potential to transform current acoustic communication systems, the study of the wavelength-scale acoustic mirage effect, an emerging field of acoustics with little prior exposure, holds great promises for realizing acoustic switches and waveguides where a tunable, curved propagation pathway is adapted to control the destination of acoustic waves.[4]

In this work, we demonstrate the wavelength-scale acoustic mirage effect using a two-dimensional (2D) gradient-index phononic crystal (GRIN PC) structure. The design of the 2D GRIN PC structure is detailed in Sec. II. By controlling the incident angle or operating frequency, the 2D GRIN PC can dynamically adjust the curved trajectory of acoustic wave propagation. We calculated the equal-frequency contours (EFCs) in each row of the GRIN PC for the shear vertical (SV)-mode bulk acoustic wave (BAW) by a plane wave expansion (PWE) method to predict the propagation trajectory of acoustic waves. In addition, we simulated SV-mode BAW propagation within the GRIN PC by a finite-difference time-domain (FDTD) method. The angular and frequency sensitivities of the acoustic mirage effect were studied. Last, we demonstrated a tunable acoustic waveguide whose guiding path can be tuned by switching working frequencies (Sec. III).

II. ACOUSTIC MIRAGE IN A GRIN PC

To introduce a tunable acoustic-velocity gradient capable of exhibiting the acoustic mirage effect on the wavelength scale, we used periodically distributed structures, called PCs, because of their ability to manipulate the wavelength-scale propagation of acoustic waves.[5,6] By varying constitutive parameters of the PCs, one can achieve complete phononic bandgaps where the propagation of acoustic waves inside the structure is forbidden.[7–13] This principle has been used to engineer acoustic waveguides by introducing straight- or bent-line defects to PCs.[14–18] In a different approach, one can employ the anisotropic properties of PCs to redirect acoustic beams in the conducting bands. It is known that when an acoustic-velocity mismatch exists between a homogeneous slab and its surrounding medium, refraction occurs at the entrance and exit interfaces of the slab. The amount of beam bending is dependent on the velocity difference, and it can be investigated through the study of EFCs in the wave-vector space. The direction of propagation is given by the group velocity of the acoustic wave beam and is normal to EFCs: $v_g = \nabla_k \omega(k)$, where ω is the angular velocity and k is the wave vector. In contrast to the circular EFCs of a homogeneous, isotropic medium, the shape of the EFCs of a PC can be highly anisotropic and frequency dependent when the acoustic wavelength is on the scale of the structure's periodicity. As a result, large bending effects such as negative refraction and self-collimation can be realized in PCs set at designated frequencies.[19–24] By calculating the effective

[a)]Author to whom correspondence should be addressed. Electronic mail: junhuang@psu.edu.

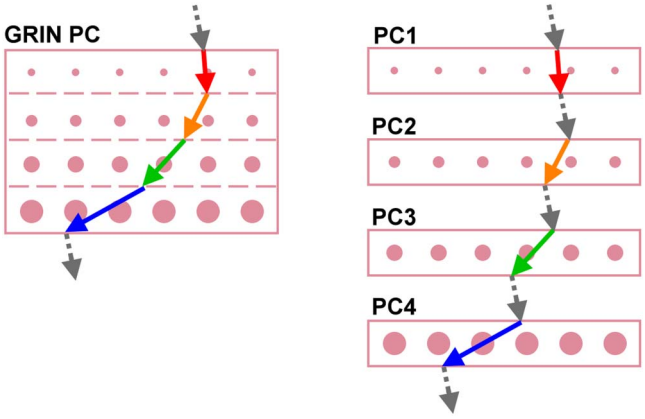

FIG. 1. (Color online) A smooth redirection of the acoustic wave propagation can be achieved by a GRIN PC where each layer can be considered an independent PC of different FR.

acoustic velocity for the propagation wave mode of a PC from its EFCs, one can readily predict the direction of refraction using Snell's law if anisotropy of the PC was negligible.[3,25,26] However, in the present PC-based applications, once the direction of refraction is determined, the refracted acoustic waves propagate along a straight line through the PC structure until entering a medium of different acoustic velocity. Thus, the existing PC-based structures cannot redirect acoustic waves continuously. In order to achieve a bent path for acoustic wave propagation, the direction of the group velocity must be successively modified during the propagation.

In this work, we demonstrate the acoustic mirage effect, continuous bending of acoustic waves along an arch-shaped trajectory, using GRIN PCs. Inspired by GRIN optics,[3,25,26] a GRIN PC (Ref. 27) is an engineered PC with a gradual variation of the constitutive parameters [e.g., filling ratios (FRs), material properties, or inclusion geometry], which produces an acoustic-velocity gradient along the variation. For example, since the band structure of a PC is highly sensitive to the variation of its FR,[24,25,27] the shape of the EFCs of a PC can be deformed by changing the inclusion radius. As a result, the acoustic velocity and refraction angle of the acoustic beam can be tuned.

As illustrated in Fig. 1, a 2D GRIN PC of a one-dimensional gradient is a discretized medium that can be thought of as a composite of multiple single-layer PCs of different FRs. When an acoustic beam propagates through a 2D GRIN PC, it encounters redirection at every virtual interface between layers, resulting in consecutive reorientations of the acoustic beam inside the structure. Thus, by gradually modulating the constitutive parameters of a GRIN PC, one may create an arc-shaped trajectory for acoustic wave propagation. The results presented in this work are restricted to an inclusion-radius gradient, but the concept can be employed for the inclusion-property or lattice-spacing gradients as well.

We first studied the effect of the FR variation on the deformation of EFCs of 2D PCs. Figure 2(a) shows the calculated band structure for the SV-mode BAW of three square-lattice PCs (PC_1, PC_2, and PC_3) with perfect periodicity, each consisting of steel cylinders embedded in epoxy.

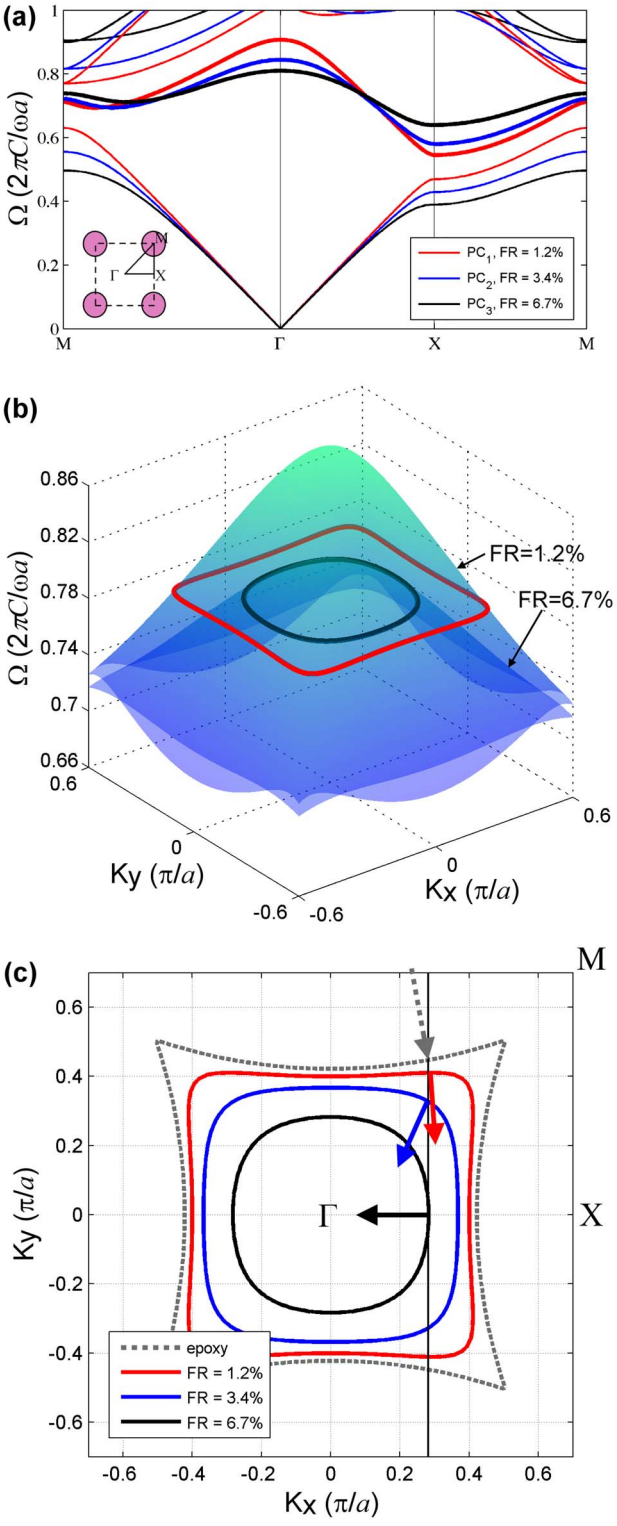

FIG. 2. (Color online) (a) Band structure for the SV-BAW mode of three PCs with FRs of 1.2% (PC_1), 3.4% (PC_2), and 6.7% (PC_3). (b) 3D dispersion curves of the second band for the SV-BAW mode of PC_1 and PC_3. The red and black curves represent the EFCs at a reduced frequency of 0.79. (c) EFCs at a reduced frequency of 0.79, for epoxy and PCs with three different FRs (1.2%, 3.4%, and 6.7%). The dotted arrow represents the incident direction. The solid line represents the construction line plotted for an incident angle of 10°. The solid arrows represent the direction of each group velocity.

Their FRs were 1.2%, 3.4%, and 6.7%, respectively. The band structure was obtained using a PWE method,[8,10,11] assuming PCs were infinitely periodic in the x and y directions while the SV-mode waves were polarized along the z direc-

tion (the cylinder axis). The frequency was reduced by a factor of $2\pi C/\omega a$, where a is the lattice spacing of the structure and C is the transverse speed of sound in epoxy. The material properties for steel were $\rho=7.78$ g/cm^3, $C_L=5.83$ km/s, and $C_T=3.23$ km/s; and those for epoxy were $\rho=1.14$ g/cm^3, $C_L=2.55$ km/s, and $C_T=1.14$ km/s, where ρ, C_L, and C_T correspond to density, longitudinal speed, and transverse speed, respectively. Figure 2(b) displays the three-dimensional (3D) dispersion curves of the second band of PC_1 and PC_3. The light (red) and dark (black) solid contours in Fig. 2(b) represent the EFCs of the PCs at a reduced frequency $\Omega=0.79$. The bell shape of the dispersion curves of both PCs implies that the group velocity pointed inwards. As the FR increased from 1.2% to 6.7%, the peak of the dispersion curve dropped and the size of the EFC decreased. As a result, the group velocity within the PC of a higher FR was greater than that within the PC of a lower FR. Figure 2(c) shows EFCs for epoxy and three square-lattice steel/epoxy PCs with FRs of 1.2%, 3.4%, and 6.7% at a reduced frequency of 0.79. The dotted arrow represents the incident acoustic beam with an angle of 10° with respect to k_y. By considering the conservation of the transverse momentum, we obtained a construction line [a thin vertical line in Fig. 2(c)] that intersected with all the EFCs. The refraction direction of the acoustic beam in each PC pointed in the direction of the inward arrow, which was normal to the EFC. It is shown that small perturbations in FR produce a large variation in the refraction angle. Hence, by steadily increasing the FR of a PC, one can alter the shape of the EFC from concave to convex, causing the acoustic beam to gradually redirect toward the center of the Brillouin zone (Γ-point).

To find an equation for the approximated curved trajectory of optical/acoustical mirage effects in nature, the Eikonal equation was used to describe the wave propagation in a piecewise isotropic medium[1]

$$\nabla n(\mathbf{u}) = \frac{d}{ds}\left[n(\mathbf{u})\frac{d\mathbf{u}}{ds}\right], \tag{1}$$

where $\mathbf{u}$ is the ray vector, n is the refractive index, and s is an elementary path length. Unfortunately, the GRIN PC discussed here would be very anisotropic when it operates in the second band of SV-BAW (Fig. 2). As a result, the acoustic mirage effect in the GRIN PC cannot be described by the Eikonal equation. However, it can be predicted from the shape of the EFC at every layer. As a GRIN PC is not strictly periodic, the constitutive properties of the structure cannot be expanded into a Fourier series using Bloch's theory, and the global dispersive properties of the whole structure cannot be obtained by the ordinary PWE method. However, for a weak gradual variation of the constitutive parameters (e.g., FR), the local dispersive properties of each row of a GRIN PC can be approximated by perfect periodic PCs. Therefore, the curved trajectory of an acoustic beam propagating in a GRIN PC can be predicted by analyzing the local EFCs of the rows consecutively crossed by the acoustic beam. Numerical simulations in the following paragraphs examined this assumption.

To numerically demonstrate this superbending phenomenon, we designed a 2D GRIN PC that was composed of

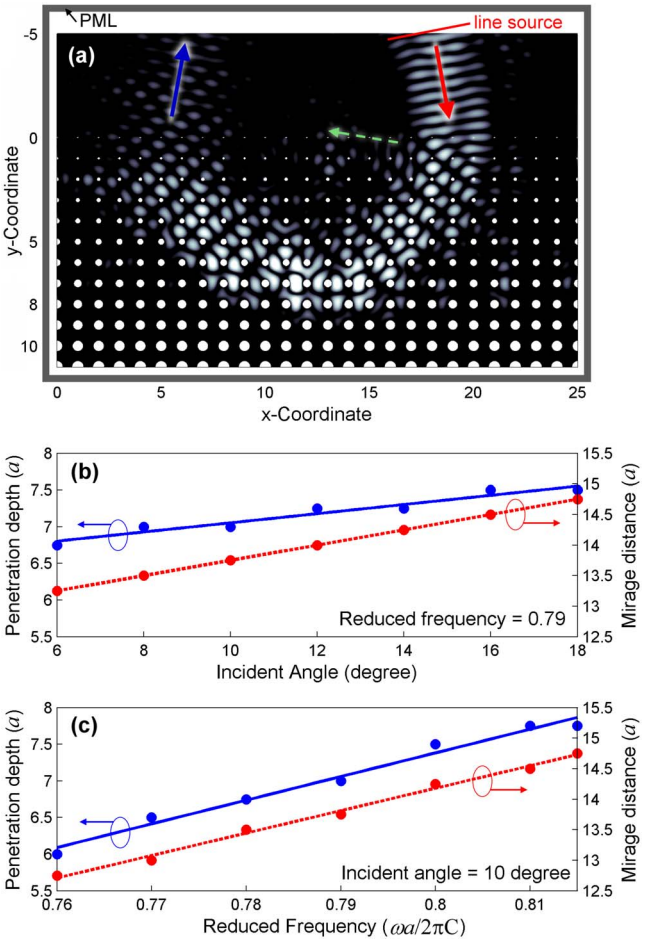

FIG. 3. (Color online) (a) "Acoustic mirage" inside a GRIN PC illuminated by a SV-mode acoustic beam with a width of $W=4a$, an incident angle of 10°, and an operating frequency of $\Omega=0.79$. The light and dark regions correspond to the strong and weak amplitudes of the displacement field, respectively. (b) The angular and (c) frequency sensitivities in a function of penetration depth and mirage distance in a GRIN PC. The solid red, solid blue, and dashed arrows denote input, output, and reflected beams, respectively.

25×12 layers of steel cylinders arranged in a square lattice and embedded in epoxy [Fig. 3(a)]. The radius of each row of cylinders increased linearly with the row number (along the y direction) per the following relation: $r_y=\sigma(y+1)a$, where $\sigma=2.08\%$. The lattice spacing was 8 mm, and the material properties were the same as those in the PWE calculations. We anticipated that the propagation of the acoustic beam inside the GRIN PC would continuously bend due to the FR gradient. To investigate the propagation of acoustic waves in the GRIN PC, we simulated the SV-mode BAW by a FDTD method.[15,28] The FDTD program was developed per the theory of elasticity: The equation of motion and the constitutive law were discretized to simulate wave propagation in linear elastic materials. A tilted line source with a width of $4a$ was placed in the epoxy region (centered at $y=-5$) and was defined by setting an initial value of body force in the equation of motion along the z axis (parallel to the cylinder axis) to generate a SV-mode BAW. Each lattice was discretized into 40 uniform spatial grids. The entire domain was surrounded by 40-grid-thick perfectly matching layers at the boundaries to avoid numerical reflections in the simulation

domain, resulting in total absorbance at the boundary.[29] To be consistent with the PWE calculations, the thermal effects on material properties[30,31] were not considered in the FDTD simulations. As shown in Fig. 3(a), the GRIN PC was exposed to an acoustic beam with an incident angle of 10° at $\Omega=0.79$ ($\lambda=a/\Omega=1.26a$). The light and dark regions represent the strong and weak amplitudes of the displacement field, respectively. The acoustic beam bent slightly toward the direction of the gradient upon entering the GRIN PC, as predicted from the EFCs [red arrow in Fig. 2(c)]. The beam then steadily refracted toward the negative x direction, redirecting back to the epoxy/GRIN PC interface with a lateral shift of $13.75a$ (equivalent to 10.9λ). The penetrating depth of the acoustic beam at the beam center, measured to be $7a$ (equivalent to 5.5λ), corresponded to a perfect periodic PC with a FR of 6.7% [the dark (black) contour in Fig. 2(b)]. While traveling within the GRIN PC structure, the beam exhibited little spread with regard to distance; however, as the beam approached the epoxy/GRIN PC interface, the width of the output beam widened marginally due to multiple reflections near the interface. A reflection beam propagating toward the negative x direction near the structure surface, denoted by the dashed arrow in Fig. 3(a), was caused by the periodicity of the epoxy/GRIN PC interface. This reflection beam interfered with the outgoing beam and resulted in the dotted shape of the output field. The transmission of displacement amplitude measured at the output was 60%, matching well with the transmission coefficient calculated from the effective acoustic impedance $Z_{\text{eff}}=Z_{\text{steel}}\text{FR}+Z_{\text{epoxy}}(1-\text{FR})$. The arc-shaped trajectory in Fig. 3(a) agrees with the directions of refraction obtained via the PWE method [Fig. 2(b)], implying that the trajectory inside a GRIN PC can be predicted by analyzing the local dispersion curves of the structure. Moreover, the results show that the GRIN PC can redirect acoustic waves within conducting bands no matter where the incident beam hits the surface. This characteristic presents a significant advantage over existing PC waveguides,[14–18] which rely on predefined line defects to guide acoustic waves within bandgaps.

III. TUNABLE ACOUSTIC WAVEGUIDE

Given that EFCs are anisotropic and frequency dependent, the propagation trajectory within a GRIN PC would be sensitive to incident angle and operating frequency. Figures 3(b) and 3(c) show how penetration depth and mirage distance (i.e., the distance between input and output beams) are dependent on incident angle and frequency, respectively. In Fig. 3(b), the angular dependences of the penetration depth and mirage distance were both linear at $\Omega=0.79$, yielding sensitivities of $0.0625a/°$ and $0.125a/°$, respectively. In contrast, the penetration depth and mirage distance have stronger dependency on the operating frequency at an incident angle of 10°, as shown in Fig. 3(c). These results demonstrated that by taking advantage of the angular or frequency sensitivity to select different trajectories within the GRIN PC, tunable acoustic waveguiding can be achieved.

To confirm the tunability of GRIN PC-based waveguiding, we simulated the propagation of acoustic waves in a modified GRIN PC with 25×17 layers. As shown in Fig. 4(a), the modified GRIN PC was symmetric with respect to the neutral axis (the horizontal dashed line along $y=8a$) while the upper part was identical to the top nine rows ($y=0-8a$) of the structure used in Fig. 3(a). For an acoustic beam operating at $\Omega=0.76$ and an incident angle of 10°, the trajectory was concave upward [Fig. 4(a)] and similar to that in Fig. 3(a). As the operating frequency was tuned to $\Omega=0.815$, however, the incident beam was negatively reflected upon crossing the epoxy/GRIN PC interface. The penetration depth increased and the acoustic beam was guided through

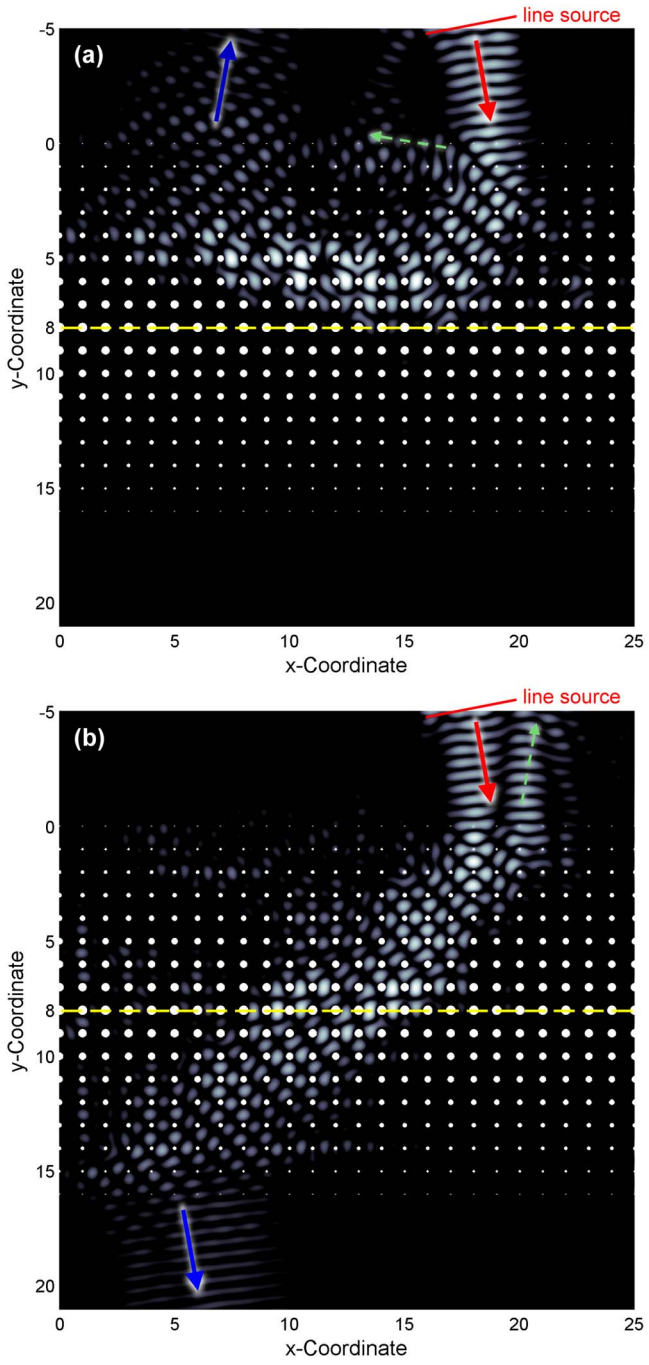

FIG. 4. (Color online) Simulated waveguiding inside a modified GRIN PC exposed to a SV-mode acoustic beam of width $W=4a$, incident angle of 10°, and reduced frequencies of (a) 0.76 or (b) 0.815. The solid red, solid blue, and dashed arrows denote input, output, and reflected beams, respectively.

the structure, as shown in Fig. 4(b). The dashed arrow denotes the reflected beam from the epoxy/GRIN PC interface that destructively interfered with the incident beam and produced a gap between the two beams. The results confirm that GRIN PC-based waveguides can dynamically control the destination of guided acoustic waves without predefined line defects; this characteristic makes GRIN PC-based waveguides useful in applications such as acoustic switching, filtering, and biosensing. Additionally, the transmission of displacement field can be improved when the structure is optimized for specific applications.

IV. SUMMARY

In conclusion, we have computationally demonstrated that the propagation direction of an acoustic wave beam within a GRIN PC can be continuously tuned by modifying the constitutive parameters of the structure. Our parametric analysis of the deformation of the dispersion curves along with FDTD studies has revealed that the acoustic mirage phenomenon can be predicted from local EFCs. We have found that the propagating trajectory of acoustic waves is sensitive to both incident angle and operating frequency. Based on these findings, we have designed an acoustic waveguide that cannot only operate without line defects, but can also be actively tuned. The methodology described in this work can be implemented in acoustic devices[32] such as on-chip waveguides, biosensors, filters, and multiplexers.

ACKNOWLEDGMENTS

The authors would like to thank Dr. T.-T. Wu and Dr. J.-H. Sun for help with the FDTD simulation, and Thomas R. Walker and Aitan Lawit for helpful discussions. They also acknowledge support from the High Performance Computing Group at the Pennsylvania State University. This research was supported by the National Science Foundation (Grant Nos. ECCS-0824183 and ECCS-0801922) and the Penn State Center for Nanoscale Science (MRSEC).

[1] C. Gómez-Reino, M. V. Perez, and C. Bao, *Gradient-Index Optics: Fundamentals and Applications* (Springer, Berlin, 2002).
[2] H. Medwin, *Sounds in the Sea: From Ocean Acoustics to Acoustical Oceanography* (Cambridge University Press, Cambridge, 2005).
[3] E. Centeno, D. Cassagne, and J.-P. Albert, Phys. Rev. B **73**, 235119 (2006).
[4] W.-P. Yang and L.-W. Chen, Smart Mater. Struct. **17**, 015011 (2008).
[5] E. Yablonovitch, Phys. Rev. Lett. **58**, 2059 (1987).
[6] M. S. Kushwaha, P. Halevi, L. Dobrzynski, and B. Djafari-Rouhani, Phys. Rev. Lett. **71**, 2022 (1993).
[7] R. E. Vines, J. P. Wolfe, and A. V. Every, Phys. Rev. B **60**, 11871 (1999).
[8] I. E. Psarobas, N. Stefanou, and A. Modinos, Phys. Rev. B **62**, 278 (2000).
[9] F. Cervera, L. Sanchis, J. V. Sánchez-Pérez, R. Martínez-Sala, C. Rubio, F. Meseguer, C. López, D. Caballero, and J. Sánchez-Dehesa, Phys. Rev. Lett. **88**, 023902 (2001).
[10] T.-T. Wu, Z.-G. Huang, and S. Lin, Phys. Rev. B **69**, 094301 (2004).
[11] V. Laude, M. Wilm, S. Benchabane, and A. Khelif, Phys. Rev. E **71**, 036607 (2005).
[12] Z. Z. Yan and Y. S. Wang, Phys. Rev. B **74**, 224303 (2006).
[13] D. Sutter-Widmer, S. Deloudi, and W. Steurer, Phys. Rev. B **75**, 094304 (2007).
[14] A. Khelif, B. Djafari-Rouhani, J. O. Vasseur, and P. A. Deymier, Phys. Rev. B **68**, 024302 (2003).
[15] J.-H. Sun and T.-T. Wu, Phys. Rev. B **74**, 174305 (2006).
[16] Y. W. Yao, Z. L. Hou, and Y. Y. Liu, J. Phys. D **39**, 5164 (2006).
[17] Y. Tanaka, T. Yano, and S. I. Tamura, Wave Motion **44**, 501 (2007).
[18] R. H. Olsson, III and I. El-Kady, Meas. Sci. Technol. **20**, 012002 (2009).
[19] S. Yang, J. H. Page, Z. Liu, M. L. Cowan, C. T. Chan, and P. Sheng, Phys. Rev. Lett. **93**, 024301 (2004).
[20] X. Zhang and Z. Liu, Appl. Phys. Lett. **85**, 341 (2004).
[21] L. Feng, X.-P. Liu, Y.-B. Chen, Z.-P. Huang, Y.-W. Mao, Y.-F. Chen, J. Zi, and Y.-Y. Zhu, Phys. Rev. B **72**, 033108 (2005).
[22] L.-S. Chen, C.-H. Kuo, and Z. Ye, Appl. Phys. Lett. **85**, 1072 (2004).
[23] A. Sukhovich, L. Jing, and J. H. Page, Phys. Rev. B **77**, 014301 (2008).
[24] J. Shi, S.-C. S. Lin, and T. J. Huang, Appl. Phys. Lett. **92**, 111901 (2008).
[25] B. K. Juluri, S.-C. S. Lin, T. R. Walker, L. Jensen, and T. J. Huang, Opt. Express **17**, 2997 (2009).
[26] X. Mao, S.-C. S. Lin, M. I. Lapsley, J. Shi, B. K. Julury, and T. J. Huang, Lab Chip **9**, 2050 (2009).
[27] S.-C. S. Lin, T. J. Huang, J.-H. Sun, and T.-T. Wu, Phys. Rev. B **79**, 094302 (2009).
[28] P.-F. Hsieh, T.-T. Wu, and J.-H. Sun, IEEE Trans. Ultrason. Ferroelectr. Freq. Control **53**, 148 (2006).
[29] J. P. Berenger, J. Comput. Phys. **114**, 185 (1994).
[30] W. K. Liu, E. G. Karpov, S. Zhang, and H. S. Park, Comput. Methods Appl. Mech. Eng. **193**, 1529 (2004).
[31] R. Yang and G. Chen, Phys. Rev. B **69**, 195316 (2004).
[32] J. Shi, X. Mao, D. Ahmed, A. Colletti, and T. J. Huang, Lab Chip **8**, 221 (2008).